

# The redshift distribution of SWIFT Gamma-Ray Bursts: evidence for evolution.

Frédéric Daigne<sup>1\*</sup>, Elena M. Rossi<sup>2†</sup> and Robert Mochkovitch<sup>1</sup>

<sup>1</sup>*Institut d’Astrophysique de Paris, UMR 7095 CNRS – Université Pierre et Marie Curie-Paris VI, 98 bd Arago, 75014 Paris, France.*

<sup>2</sup>*JILA, University of Colorado, Boulder, CO 80309-0440, USA*

Accepted \*\*.\*\*.\*\*\*; Received \*\*.\*\*.\*\*\*; in original form \*\*.\*\*.\*\*\*.

## ABSTRACT

We predict the redshift distribution of long Gamma-Ray Bursts (GRBs) with Monte Carlo simulations. Our improved analysis constrains free parameters with three kinds of observation: (i) the  $\log N - \log P$  diagram of BATSE bursts; (ii) the peak energy distribution of bright BATSE bursts; (iii) the HETE2 fraction of X-ray rich GRBs and X-ray flashes. The statistical analysis of the Monte Carlo simulation results allow us to carefully study the impact of the uncertainties in the GRB intrinsic properties on the redshift distribution. The comparison with SWIFT data then leads to the following conclusions. The Amati relation should be intrinsic, if observationally confirmed by SWIFT. The progenitor and/or the GRB properties have to evolve to reproduce the high mean redshift of SWIFT bursts. Our results favor an evolution of the efficiency of GRB production by massive stars, that would be  $\sim 6 - 7$  times higher at  $z \sim 7$  than at  $z \sim 2$ . We finally predict around 10 GRBs detected by SWIFT at redshift  $z > 6$  for a three year mission. These may be sufficient to open a new observational window over the high redshift Universe.

**Key words:** gamma-rays: bursts – stars: formation – cosmology: observations.

## 1 INTRODUCTION

Gamma-ray bursts (hereafter GRBs) are powerful flashes of high-energy photons, that travel undisturbed from cosmological distances to earth, where they can be easily detected. Therefore, independently of their physical origin, GRBs can be used to probe the distant Universe (Lamb & Reichart 2000; Blain & Natarajan 2000; Totani 1999; Wijers et al. 1998). In addition, there has recently been growing observational evidence that long GRBs occur in star-forming regions (Bloom et al. 2001) and that some of them are associated with peculiar type Ic supernova explosions, i.e. with massive progenitors (e.g. Galama et al. 1998; Stanek et al. 2003; Hjorth et al. 2003; Malesani et al. 2004). The possible detection of GRBs at cosmological distance and their association with massive stars motivate two questions: (i) how is the long GRB rate related to the star formation rate (SFR) ? (ii) what is the expected detection rate of long GRBs at high redshift ? On the one hand, a better understanding of the first issue is a necessary step to be able to use GRBs to directly trace the star formation history in the universe. Observations give strong indications in favor of an association of long GRBs with

massive stars. However, the actual physical conditions (e.g. mass, metallicity, rotation, binarity) for a star to trigger a burst are not currently known. Thus the GRB and star formation rates may be related in a non trivial way. On the other hand, GRBs could be produced in the Universe in association with first stars and are thus expected up to very high redshifts (e.g. Bromm & Loeb 2005). Therefore, they are potentially important tools of investigation of the cosmic evolution; they are probably unique direct probe at  $z \gtrsim 6.5$ . First, the afterglow emission may be used to study the ionization and metal enrichment histories of the intervening intergalactic medium (e.g. Chen et al. 2006). Then, they can give insight into galaxy formation and evolution: they allow us to detect very faint galaxies at high redshift, that otherwise would have eluded detection (e.g. Berger et al. 2006). In turn, the detection of high redshift galaxies can better constrain the SFR where current results are most uncertain. Finally, they might be important to constrain the small-scale power spectrum of primordial density fluctuations (Mesinger et al. 2005).

The standard approach to investigate such questions is to assume a GRB comoving rate, luminosity function and spectrum (e.g. Porciani & Madau 2001, thereafter PM01) and to constrain the free parameters of the model by observed data, especially the GRB  $\log N - \log P$  diagram

\* E-mail: daigne@iap.fr

† Chandra Fellow

(Schmidt 1999). We follow this approach, by the mean of Monte Carlo simulations. Such an approach allows a realistic parametrization of the intrinsic GRB properties, a more accurate treatment of detection criteria for several instruments and a study of the impact of the uncertainties in the GRB physics on the predicted GRB rate. Compared to previous studies (Lamb & Reichart 2000, PM01, Firmani et al. 2004; Guetta et al. 2005; Natarajan et al. 2005), we add two more observational constraints that allow us to better determine the model parameters: the observed peak energy distribution of bright BATSE bursts and the fraction of X-ray rich GRBs (hereafter XRRs) and X-ray flashes (hereafter XRFs) in the HETE2 GRB sample. Together with the data obtained during SWIFT first year, this method allows us to address the two questions that motivated this work.

The paper is organized as follows. In section 2, we describe our assumptions on the GRB intrinsic properties (comoving rate, luminosity and spectrum). Then, we describe our Monte Carlo simulations in section 3. We especially detail our detection criteria for several instruments (BATSE, HETE2 and SWIFT) and the observations we use to constraint the free parameters of the model. Our results are discussed in section 4 and section 5 is the conclusion.

## 2 GRB INTRINSIC PROPERTIES

Our Monte Carlo simulations are necessarily based on some assumptions regarding the GRB intrinsic properties. In some cases, the large uncertainties in these properties lead us to consider several scenarios. In this way, we can study the impact of this poor physical understanding of the GRB phenomenon on our predictions, especially on the GRB redshift distribution.

### 2.1 Comoving rate

Searching for high redshift galaxies has extended the number of rest frame UV-bright systems over the interval  $0 \leq z \lesssim 10$  (e.g. Giavalisco et al. 2004; Bouwens et al. 2005). These data have been used to probe the redshift evolution of the SFR. It seems established that the SFR density grows by an order of magnitude from  $z = 0$  to  $z \sim 1$  and levels off around  $z \simeq 2$  (see Hopkins (2004) and Fig. 1, for a recent collection of data). The shape of the star formation history is more uncertain for  $z > 3$ . Recent investigations of photometric dropouts at  $z \gtrsim 6$  suggest a strong decline of more than an order of magnitude from  $z = 3$  to  $z \sim 10$  (Bouwens et al. 2003, 2005; Fontana et al. 2003; Stanway et al. 2004). However, the assessment of this result is subject to the poorly constrained dust obscuration at such high redshifts.

Since long GRBs are very likely related to the death of massive stars, the most simple assumption is to adopt a GRB rate proportional to the SFR. Following PM01, we take

$$\mathcal{R}_{\text{GRB}} = k \times \mathcal{R}_{\text{SN}} , \quad (1)$$

where  $\mathcal{R}_{\text{GRB}}$  is the GRB comoving rate and  $\mathcal{R}_{\text{SN}}$  is the type

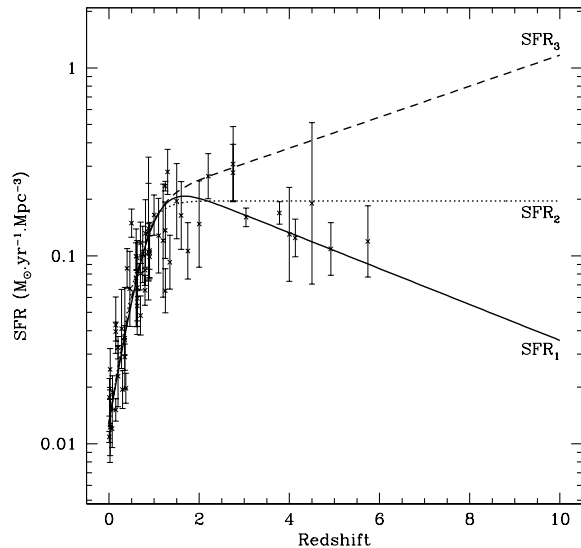


**Figure 1.** The three star formation rates considered in this paper. Observed data are taken from Hopkins (2004).

II supernova comoving rate. We assume the same initial mass function (IMF) as in PM01. As this IMF is constant with time, the supernova rate is proportional to the SFR :

$$\mathcal{R}_{\text{SN}} = 0.0122 M_{\odot}^{-1} \times \text{SFR} , \quad (2)$$

the lifetime of massive stars being neglected. We first considered for the SFR a simple fit of observed data up to  $z \sim 6$  (Hopkins 2004). This case is thereafter called SFR<sub>1</sub>. As the true evolution of the SFR above  $z \sim 2-3$  is still uncertain, we have also considered two alternative rates : SFR<sub>2</sub>, where the SFR is constant above  $z \sim 2$  and SFR<sub>3</sub>, where the SFR still increases above  $z \sim 2$ . In this last case, we arbitrarily cut the GRB rate at  $z_{\text{max}} = 20$ . These three SFRs are plotted in Fig. 1. They are in fact very close to those adopted by PM01. Lamb & Reichart (2000) considered two cases, one being close to SFR<sub>1</sub> and one being close to SFR<sub>2</sub> with an additional very intense component at  $z \gtrsim 6-7$ . The preferred SFR in the results by Natarajan et al. (2005) is close to our SFR<sub>3</sub> up to  $z \sim 6-7$ . Finally Firmani et al. (2004) adopted a rather different approach. The SFR in their study is a three free parameters function. It is adjusted together with the luminosity function under the joint constraint of the BATSE  $\log N - \log P$  diagram and the “observed” GRB redshift distribution provided by the luminosity-variability relation (Fenimore & Ramirez-Ruiz 2000).

The ratio of GRB explosions to type II supernovae,  $k$ , is a free parameter of the model. Here  $\mathcal{R}_{\text{GRB}}$  has to be understood as the comoving rate of GRBs pointing towards us. The true GRB rate in the Universe (as well as the true GRB / SN ratio) is obtained by multiplying this rate by a correcting factor for the beaming, which is of the order of  $\langle (\Omega/4\pi)^{-1} \rangle \sim 500 - 1000$  (Frail et al. 2001).

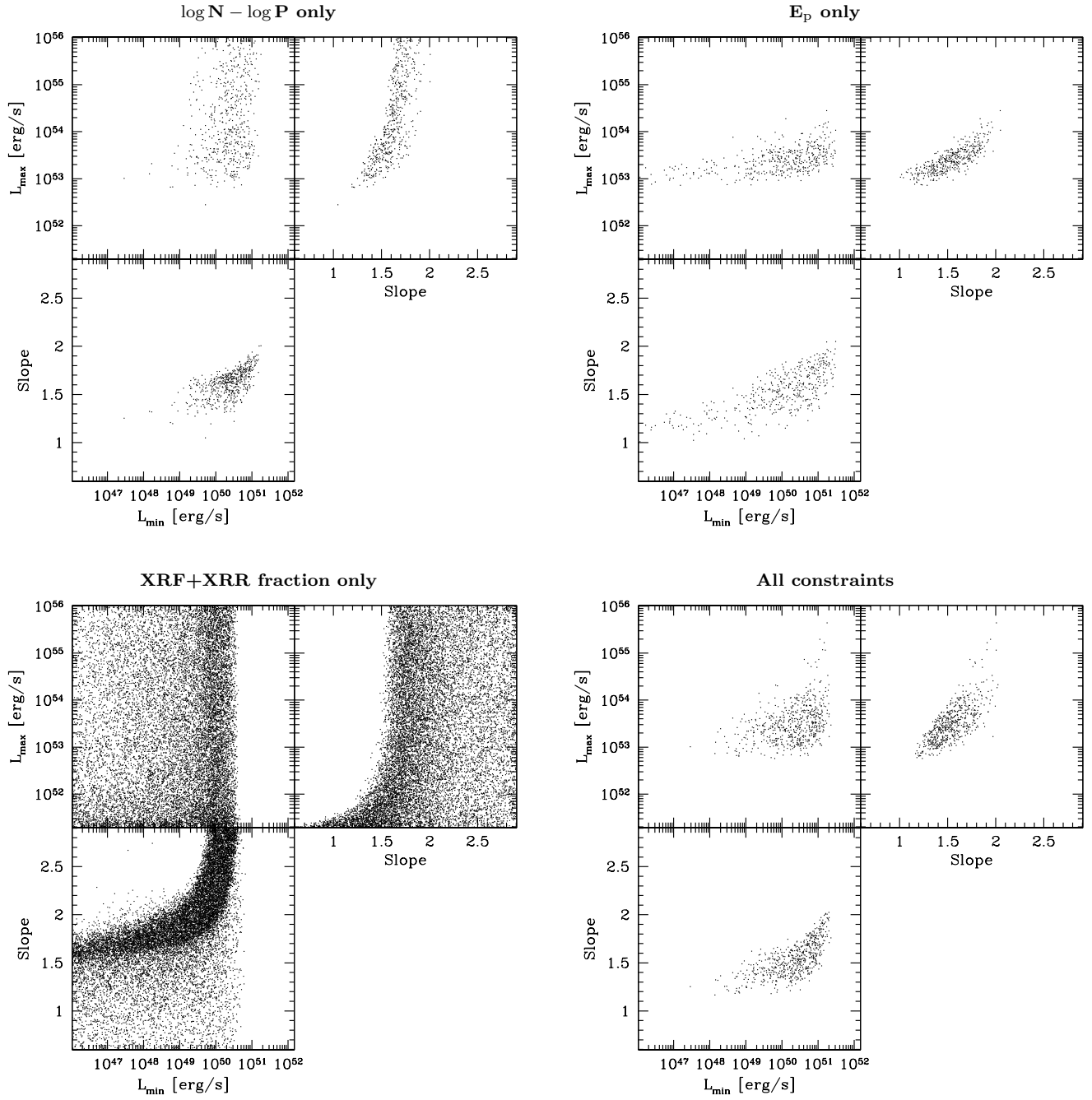


**Figure 2. Parameter space (SFR<sub>3</sub>, Amati-like relation)** : we plot the location in the parameter space of the best models (see section 3.3). *Top-left*: models that fit the BATSE  $\log N - \log P$  diagram (Stern et al. 2000, 2002); *Top-right*: models that fit the peak energy distribution of bright BATSE bursts (Preece et al. 2000); *Bottom-left*: models that fit the fraction of XRFs and XRRs observed by HETE2 (Sakamoto et al. 2005); *Bottom-right*: models that fit the three constraints.

## 2.2 Luminosity function

The GRB luminosity function is currently quite uncertain. We assume a power-law distribution, which does not vary with redshift:

$$p(L) \propto L^{-\delta} \text{ for } L_{\min} \leq L \leq L_{\max} . \quad (3)$$

Notice that  $p(L)$  is the distribution of the isotropic equivalent luminosity of GRBs that would be obtained by a perfect (no threshold) detector on Earth. This is of course different from the true distribution of  $L$  for all GRBs in the Universe, which could be obtained from  $p(L)$  after correction for viewing selection effects. With  $p(L)$  there are three more model parameters: the slope  $\delta$  and the minimum and maximum luminosities  $L_{\min}$  and  $L_{\max}$ . Previous studies also used such

a power-law luminosity function (Lamb & Reichart 2000) or a Schechter luminosity function (PM01, Natarajan et al. 2005). This latter is very close to a single power-law extending to  $L_{\max} = +\infty$  with an additional low-luminosity tail below  $L_{\min}$  that does not contribute much due to an exponential cutoff. Firmani et al. (2004) also used a power-law distribution, but including the additional possibility that the typical GRB luminosity scales with  $(1+z)^\nu$  with  $\nu \sim 0.8 - 1.2$ . We also briefly tested such evolutionary effect (see section 4.1).

### 2.3 Spectrum

The intrinsic photon spectrum is assumed to be a broken power-law with a break at energy  $E_p$  (Band et al. 1993) and a low (resp. high) energy slope  $-\alpha$  (resp.  $-\beta$ ). We checked that a more realistic spectrum shape, the so-called ‘‘GRB’’ function (Band et al. 1993), has only a small impact on our results and does not affect our conclusions. The probability distributions of the low-energy and high-energy slopes follows the observed distribution of  $\alpha$  and  $\beta$  in a set of long bright GRBs (Preece et al. 2000). We have checked a posteriori that the simulated distributions of the ‘‘observed’’ low- and high-energy slopes in long bright GRBs were very close to the intrinsic distributions.

As the observed peak energy distribution of these same bright burst is close to log-normal (Preece et al. 2000), the most simple assumption is to adopt an intrinsic log-normal distribution for  $E_p$ , with a dispersion  $\sigma$  and a mean value  $E_{p,0}$ . This is our first scenario (hereafter ‘‘log-normal  $E_p$  distribution’’). We assume  $\sigma = 0.3$  dex (we checked that our results do not depend too much on this assumption) and we keep  $E_{p,0}$  as a free parameter. On the other hand, there are some evidences that the intrinsic peak energy could be correlated with the intrinsic luminosity. Therefore, we have considered a second scenario (hereafter ‘‘Amati-like relation’’), where

$$E_p = 380 \text{ keV} \left( \frac{L}{1.6 \times 10^{52} \text{ erg s}^{-1}} \right)^{0.43}, \quad (4)$$

with a normal dispersion  $\sigma = 0.2$  dex, in agreement with the observed relation (Yonetoku et al. 2004; Ghirlanda et al. 2005, see however Nakar & Piran 2005; Band & Preece 2005 who tested this relation against BATSE data and concluded that selection effects were dominant). In this second scenario, no free parameter is introduced for the spectrum.

Notice that the treatment of the spectrum in this work is improved compared to previous studies: Lamb & Reichart (2000) adopted a single power-law spectrum of slope  $\alpha = -1$  which of course is a very poor approximation for high redshift GRBs. Other studies (PM01, Firmani et al. 2004; Natarajan et al. 2005) adopt a standard GRB spectrum with fixed slopes  $\alpha = -1$  and  $\beta = -2.25$  and a constant break energy  $E_b$  in the GRB rest frame which is a priori fixed to 511 keV ( $E_p = E_b \times (2+\alpha)/(\alpha-\beta) \sim 410$  keV in the GRB rest frame), without any a posteriori check that the simulated observed  $E_p$  distribution is in agreement with BATSE data. Firmani et al. (2004) also consider a case including an intrinsic Amati-like relation of slope 0.5, but without any dispersion.

**Table 1. Best models: parameters.**

SFR	$\log L_{\min}$	$\log L_{\max}$	$\delta$	$\log k$
<b>Amati-like relation <math>E_p \propto L^{0.43}</math></b>				
<b>1</b>	$49.9 \pm 0.5$	$53.7 \pm 0.4$	$1.70 \pm 0.08$	$-5.4 \pm 0.3$
<b>2</b>	$50.0 \pm 0.5$	$53.7 \pm 0.5$	$1.68 \pm 0.10$	$-5.5 \pm 0.3$
<b>3</b>	$50.3 \pm 0.7$	$53.5 \pm 0.4$	$1.54 \pm 0.18$	$-6.0 \pm 0.2$
<b>log-normal distribution peak energy distribution</b>				
<b>1</b>	$50.2 \pm 0.9$	$53.6 \pm 0.8$	$1.62 \pm 0.18$	$-5.6 \pm 0.3$
<b>2</b>	$50.2 \pm 1.1$	$53.6 \pm 0.9$	$1.62 \pm 0.27$	$-5.7 \pm 0.3$
<b>3</b>	$50.5 \pm 1.3$	$53.7 \pm 0.9$	$1.52 \pm 0.48$	$-6.2 \pm 0.2$
<b>SFR <math>\log E_{p,0}</math></b>				
<b>log-normal distribution peak energy distribution</b>				
<b>1</b>	$2.74 \pm 0.08$			
<b>2</b>	$2.73 \pm 0.08$			
<b>3</b>	$2.79 \pm 0.08$			

### 3 MONTE CARLO SIMULATIONS

In our Monte Carlo simulations, each generated GRB is given a redshift, a luminosity and a spectrum, according to the specific intrinsic distributions that have been described above. Then observed properties (observed peak energy, peak flux) can be computed and compared to the sensitivity of different instruments. In this study, we focus on BATSE, HETE2 and SWIFT. Our detection criteria are specified in section 3.1. This allows us to derive the expected distributions of observed redshifts, peak fluxes and peak energies for these instruments, for comparison with real data. It also allows to reconstruct the source frame properties (e.g. luminosity, peak energy) of detected bursts. In a second step, the free parameters of the model are adjusted to fit several observational constraints. This is explained in section 3.2.

#### 3.1 Detection criteria

We consider the detection by three instruments: BATSE, HETE2 and SWIFT. For BATSE, we apply the detection efficiency as a function of the peak flux,  $\epsilon(P)$ , given by Kommers et al. (2000), so that we can compare our results with the  $\log N - \log P$  diagram published by these authors. We also compare our simulated bursts with the  $\log N - \log P$  diagram published by Stern et al. (2000, 2002). Their sample goes farther towards low flux bursts and puts therefore more constraints on the GRB rate at high redshift. Their published diagram is already corrected for detection efficiency. In addition we apply a threshold  $P_{50-300 \text{ keV}} > 5 \text{ ph cm}^{-2} \text{ s}^{-1}$  defining a sub-sample of ‘‘bright BATSE bursts’’, to compare our simulated GRBs with the results of the BATSE spectroscopic catalog (Preece et al. 2000). In our simulations, this threshold typically corresponds to 5 % to 10 % of BATSE bursts, in agreement with observations. For HETE2, we adopt the same threshold of  $1 \text{ ph cm}^{-2} \text{ s}^{-1}$  both for the WXM (2-10 keV) and for FREGATE (30-400 keV) (J.L. Atteia, private communication).

Swift uses two detection modes: one based on a flux

**Table 2. Best models: mean redshift.**

Rate	All	SWIFT	Bright SWIFT
<b>Amati-like relation <math>E_p \propto L^{0.43}</math></b>			
SFR1	3.1	1.6	1.3
SFR2	8.0	1.9	1.5
SFR3	10.5	3.3	2.1
<b>log-normal peak energy distribution</b>			
SFR1	3.1	1.9	1.6
SFR2	8.0	2.4	1.8
SFR3	10.5	4.8	2.7

threshold and one on fluence threshold (image mode). The post-launch analysis can be found in Band (2006). We use his results to define a detection probability at peak flux  $P_{15-150 \text{ keV}}$ , based on the observed GRB duration distribution. The mean flux threshold is  $\sim 0.2 \text{ ph cm}^{-2} \text{ s}^{-1}$ . We also defined a sub-sample of “bright SWIFT bursts” by selecting bursts with peak flux  $P_{15-150 \text{ keV}} > 1 \text{ ph cm}^{-2} \text{ s}^{-1}$ .

### 3.2 Observational constraints

Depending on the assumption for the intrinsic peak energy distribution, our model has four (Amati-like relation) or five (log-normal  $E_p$  distribution) free parameters. These parameters can be constrained by the following observations: (1) the  $\log N - \log P$  diagram of BATSE bursts (Kommers et al. 2000; Stern et al. 2000, 2002). (2) the observed peak energy distribution of long bright GRBs (Preece et al. 2000) (3) the observed fraction of XRRs and XRFs in the sample of GRBs detected by HETE2. We adopt the same definitions as the HETE2 team for these sub-classes, as well as their published observed ratio (Sakamoto et al. 2005).

Combining those three observations, we get 41 data points, so that our model has 37 (resp. 36) degrees of freedom in the Amati-like relation scenario (resp. the log-normal  $E_p$  distribution scenario). We find the best fit parameters and their dispersion by  $\chi^2$  minimization, as detailed below.

### 3.3 Parameter determination

We consider the six cases corresponding to our three assumed SFRs and our two possible spectral scenarios. In each case, we are able to find a good fit to the data. The search for the best fit is made by randomly choosing  $L_{\min}$  (resp.  $L_{\max}$ ) in the interval  $10^{46}-10^{52} \text{ erg s}^{-1}$  (resp.  $10^{51}-10^{56} \text{ erg s}^{-1}$ ),  $\delta$  in the range 0.5-3 and by adjusting the normalization  $k$  to minimize the  $\chi^2$ . More than  $10^5$  sets of parameters are tried for each of the six scenarios, and more than  $10^5$  GRBs are simulated in the Monte Carlo run for each of these sets. For each case, we define “best models” as models that fit the three observational constraints at the 1 sigma level, i.e. models for which  $\chi_{\min}^2 \leq \chi^2 \leq \chi_{\min}^2 + \Delta\chi^2$ , with  $\Delta\chi^2 = 40.5$  (resp. 39.5) for 37 degrees of freedom (resp. 36). We can then compute the mean value and the dispersion of the best model parameters, as well as of any function of these parameters, such as the predicted SWIFT GRB redshift distribution. An example is given in Fig. 2 in the case SFR<sub>3</sub>

**Table 3. Best models: predicted fraction of all and bright SWIFT GRBs above  $z = 6$  and  $z = 7$ .** The reported values are averaged over all “best models”. The uncertainty in each case can be estimated from Fig. 4.

Rate	SWIFT		Bright SWIFT	
	$\%(z > 6)$	$\%(z > 7)$	$\%(z > 6)$	$\%(z > 7)$
<b>Amati-like relation <math>E_p \propto L^{0.43}</math></b>				
SFR1	0.7%	0.4%	0.3%	0.1%
SFR2	2.5%	1.6%	0.8%	0.4%
SFR3	15%	12%	2.0%	1.8%
<b>log-normal peak energy distribution</b>				
SFR1	1.4%	0.7%	0.6%	0.3%
SFR2	4.5%	2.9%	1.6%	1.0%
SFR3	21%	17%	6.2%	4.5%

+ Amati-like relation. Very similar plots are obtained in all the other considered cases. In the top-left panel of Fig. 2, we show the location of the best models in the parameter space  $L_{\min}-L_{\max}-\delta$ , using the  $\log N - \log P$  constraint only. It clearly appears that this constraint can fix the slope  $\delta$  of the luminosity function but leaves a degeneracy on  $L_{\min}$  and  $L_{\max}$ . Adding the two other constraints improve the parameter determination (top-right, bottom-left panels in Fig. 2). Indeed, it can be seen that  $L_{\max}$  is better constrained using the peak energy distribution of bright BATSE bursts. The uncertainty on  $L_{\min}$  is slightly reduced using the third constraint. Finally the comparison between the top-left panel ( $\log N - \log P$  only) and the bottom-right panel (three constraints together) shows the improvement in the parameter determination given by our method.

In all considered cases, we always find a clear minimum for  $\chi^2$ . As expected, we also find that for each physical quantity, the mean value for the best models defined as above is very close to the value for the minimum  $\chi^2$  model. The quality of the best fit can be seen in Fig. 3. Finally the results are shown in Table 1, where we indicate for each case the mean value and the dispersion of the best model parameters. The obtained error bars confirm that the slope of the luminosity function remains better determined than the minimum and maximum luminosities.

## 4 RESULTS AND DISCUSSION

### 4.1 Redshift distribution

For each scenario, we report in Table 2 the mean redshift we obtain for all GRBs (intrinsic mean redshift), all GRBs detected by SWIFT and bright GRBs detected by SWIFT. The corresponding redshift distributions are plotted in Fig. 4, as well as the observed distribution for SWIFT bursts (Jakobsson et al. 2006). Each simulated redshift distribution is computed averaging over the “best models”. The computed dispersion around this mean is the hatched region in Fig. 4.

The observed redshift distribution of SWIFT bursts is plagued by selection effects, difficult to account for. For example, the deficiency of low redshift ( $z \sim 1$ ) events, with respect to pre-SWIFT bursts (see fig.3 in Jakobsson et al.

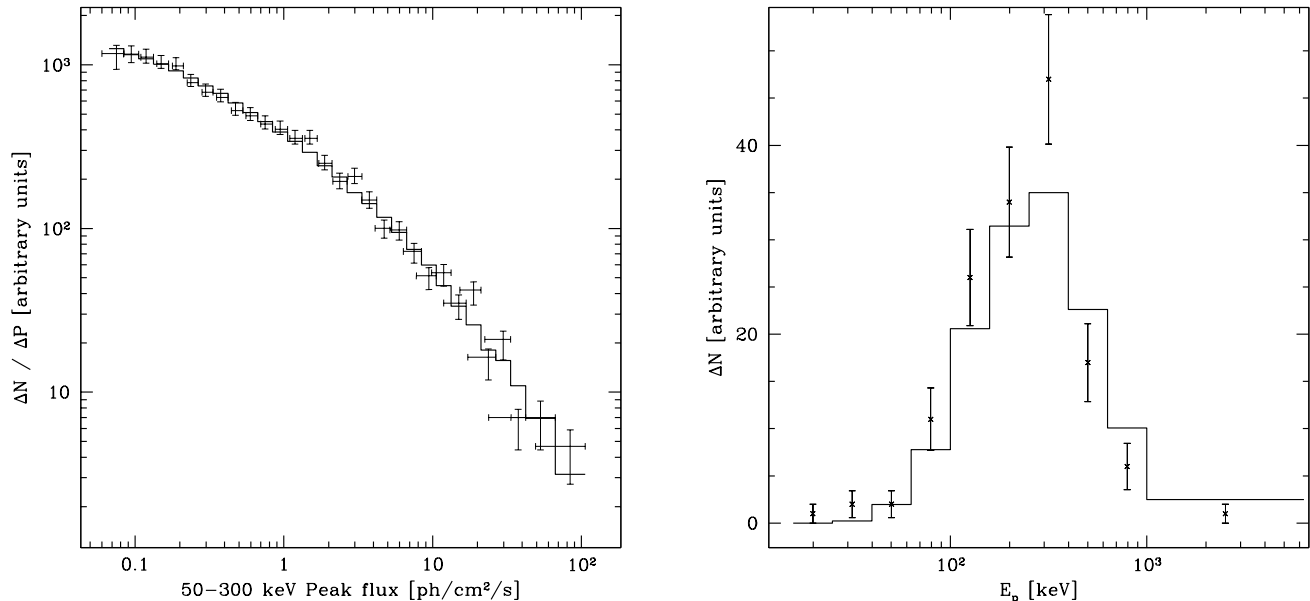


**Figure 3. Best model (SFR<sub>3</sub>, Amati-like relation)**. *Left*: the simulated  $\log N - \log P$  diagram of BATSE bursts is plotted as well as BATSE data (Stern et al. 2000, 2002); *right*: the simulated peak energy distribution of bright BATSE bursts is plotted as well as the observed distribution (Preece et al. 2000).

2006) is not yet understood. For this reason, we do not attempt a formal fit of the data. However, we expect the observed distribution to be located between the simulated distributions of all SWIFT bursts (thin hatched region in fig. 4) and of “bright” SWIFT bursts, with peak flux above  $1 \text{ ph cm}^{-2} \text{ s}^{-1}$  in the 15-150 keV band (thick hatched region). Figure 4 clearly shows that the expected redshift distribution strongly depends on the assumption made on the GRB comoving rate, so that SWIFT data can already put severe constraints on this rate. The case SFR<sub>1</sub> illustrates the effect of instrument thresholds: with a mean redshift  $\langle z \rangle \sim 1.3 - 1.9$ , the simulated redshift distribution of bursts detected by SWIFT is very far from the observed one ( $\langle z \rangle \sim 2.8$ ; Jakobsson et al. 2006), despite an intrinsic distribution of all GRBs that is much closer. Similarly SFR<sub>2</sub> gives a lower mean redshift ( $\langle z \rangle \sim 1.5 - 2.4$ , see table 2) than the observed one. Conversely, SFR<sub>3</sub> gives a much better agreement with data ( $\langle z \rangle \sim 2.1 - 4.8$ ). The observed SWIFT distribution lies just between the simulated redshift distribution of all SWIFT bursts and that of bright SWIFT bursts, as expected. This is qualitatively in agreement with the analysis performed by Jakobsson et al. (2006) who found that SWIFT data were better reproduced using Model II of Natarajan et al. (2005), which corresponds to a SFR still rising up to  $z \sim 7$ , i.e. close to our SFR<sub>3</sub>. Our results seem rather independent on the details of the intrinsic GRB properties, as the Amati-like relation and the log-normal  $E_p$  give very similar distributions.

We provide in addition in Table 3 the predicted fraction of all and bright SWIFT bursts above  $z = 6$  and  $z = 7$ . We find that this fraction is less than 1 % for SFR<sub>1</sub>. Assuming 100 SWIFT GRBs per year, we expect less than 5 GRBs per year above  $z = 6$  for SFR<sub>2</sub> (resp. less than 2 bright

GRBs per year). In this case, most high redshift GRBs will be located around  $z = 6 - 7$ . In the SFR<sub>3</sub> case, we expect 15-20 SWIFT GRBs per year above  $z = 6$ , including 2-6 bright GRBs. In this case, a non negligible fraction of GRBs is predicted above  $z = 7$ . Clearly, the detection of GRB 050904 at  $z = 6.29$  during the first year of SWIFT (Kawai et al. 2006) is very unlikely with SFR<sub>1</sub>, marginally compatible with SFR<sub>2</sub> and more easily explained with SFR<sub>3</sub>.

The fact that SFR<sub>3</sub> seems preferred by data is quite surprising, as this SFR is probably unrealistic: such a high rate of star formation at large redshift would result in an intense production of metals that would lead to much higher metallicities in the structures and in the IGM than observed (see e.g. Daigne et al. 2004, 2005). Therefore, our results provide strong evidence that the properties of GRBs or/and GRB-progenitors are redshift dependent.

One possibility is that the efficiency of GRB production by stars decreases with time. The ratio  $k$  of GRBs over type II supernovae would thus increase with redshift. If the true cosmic SFR in the Universe is more similar to SFR<sub>1</sub> (resp. SFR<sub>2</sub>), then our results show that this efficiency at  $z \sim 6 - 7$  is  $\sim 6 - 9$  (resp.  $\sim 2 - 3$ ) higher than at  $z \sim 2$  (see Fig. 1). There is indeed increasing observational evidence that the GRB rate does not directly trace the SFR (Le Floc’h et al. 2006). Such an evolution could be related to many factors: metallicity, mass, rotation, or binarity of the progenitors.

On the other hand, there could be an evolution of GRB intrinsic properties with time (e.g. more luminous GRBs at large redshift). We tested the impact of a GRB luminosity evolution by considering a model where  $L_{\min}$  and  $L_{\max}$  scale as  $(1+z)^\nu$ , the slope of the luminosity function being kept constant. We found that it is possible to reconcile SFR<sub>1</sub> with

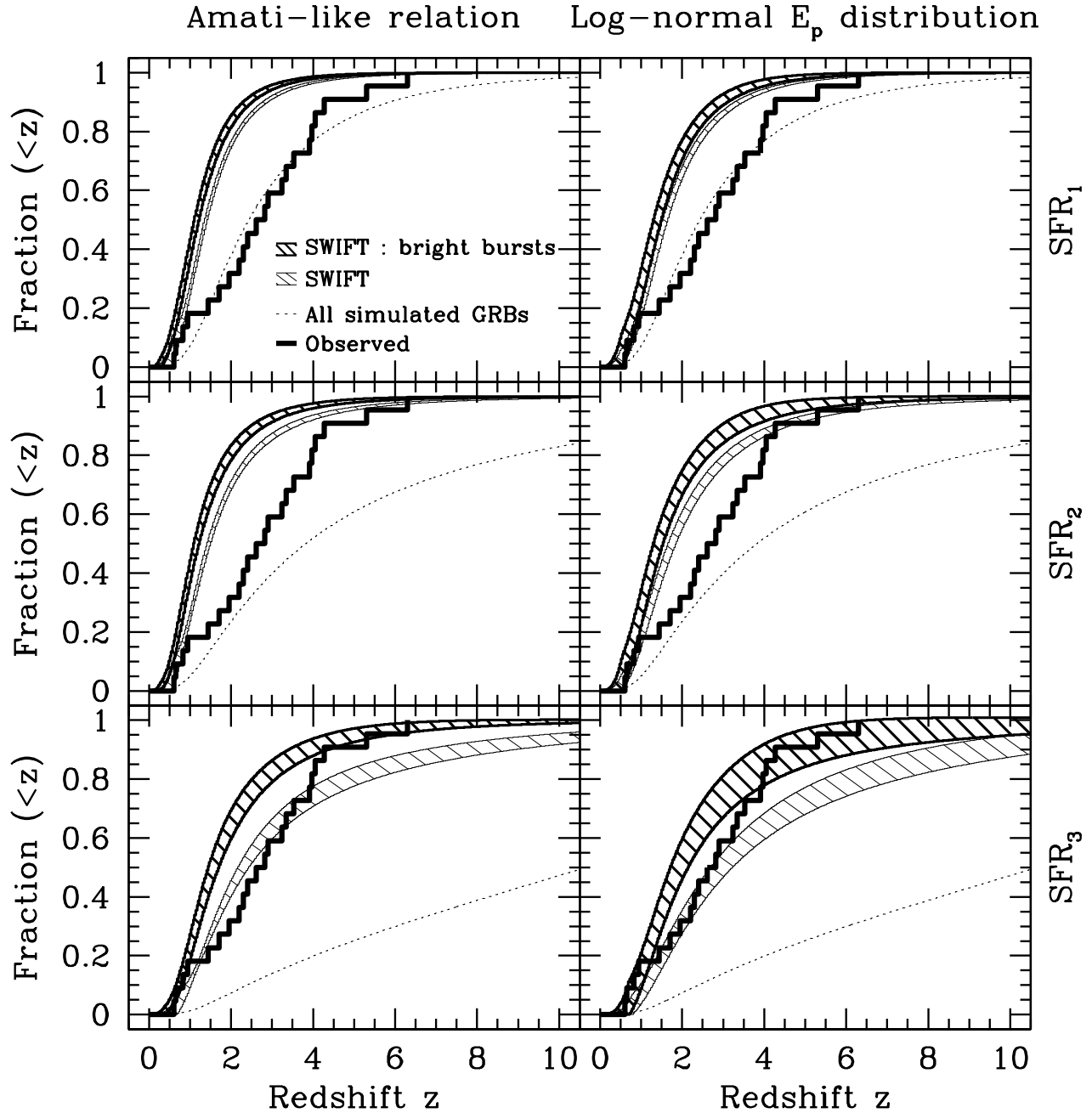


**Figure 4. Best models: redshift distribution.** Each diagram shows for the six considered cases (1) the observed distribution of SWIFT bursts with measured redshifts (thick line); (2) the redshift distribution of all simulated bursts (thin dotted line); (3) the redshift distribution of simulated bursts that are detected by SWIFT (thin hatched region); (4) the redshift distribution of bright SWIFT bursts (thick hatched region).

SWIFT data but this would imply a very strong evolution ( $\nu > 2$ ), probably unrealistic. However, it is unlikely that progenitor characteristics would evolve without any changing in the GRB properties. Therefore, we suspect that both evolutionary effects are, in fact, present but that our results are mostly due to the former.

#### 4.2 Luminosity function and peak energy distribution

The Amati-like relation scenario and the log-normal  $E_p$  distribution scenario lead to rather similar redshift distribution but differ strongly in some other aspects: (i) as can be seen in Fig. 5 (right panel), selection effects only can not create an apparent Amati-like correlation between the luminosity and the intrinsic peak energy when it is not originally

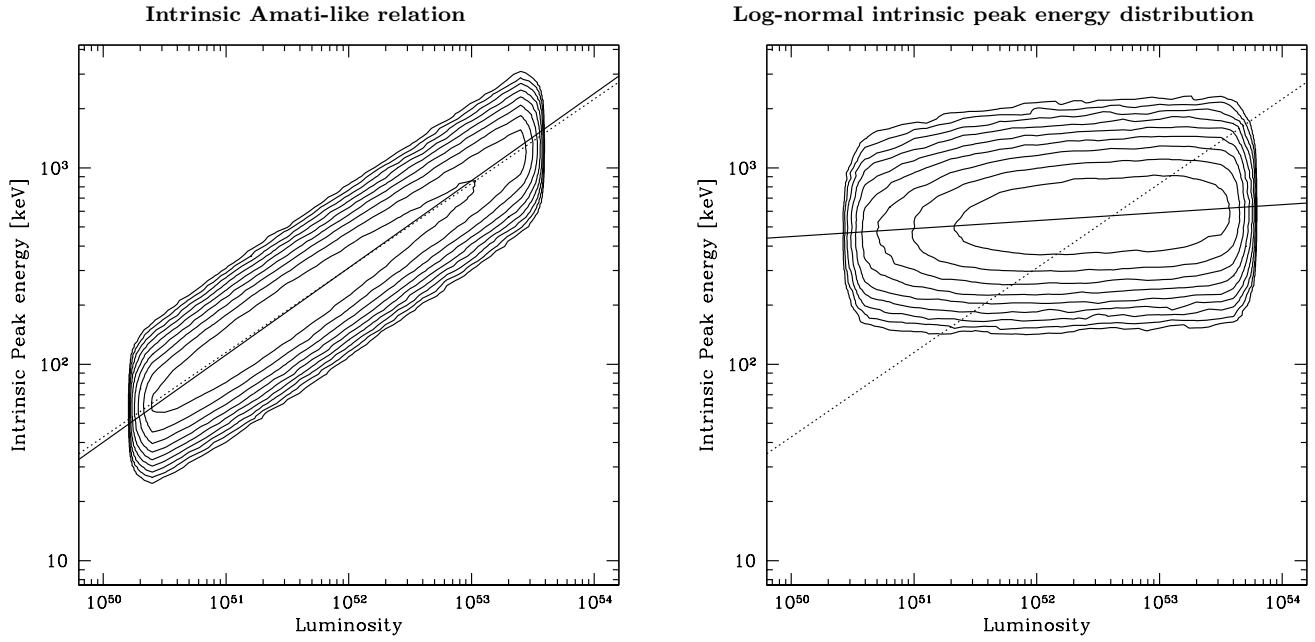


**Figure 5. Amati-like relation in the best model ( $SFR_3$ ).** GRB density contours are plotted in the luminosity-intrinsic peak energy plane for SWIFT bursts. The slope is indicated in solid line, as well as the observed slope in dotted line (Ghirlanda et al. 2005). *Left* : simulation using an intrinsic Amati-like relation; *right* : simulation where the intrinsic peak energy follows a log-normal distribution.

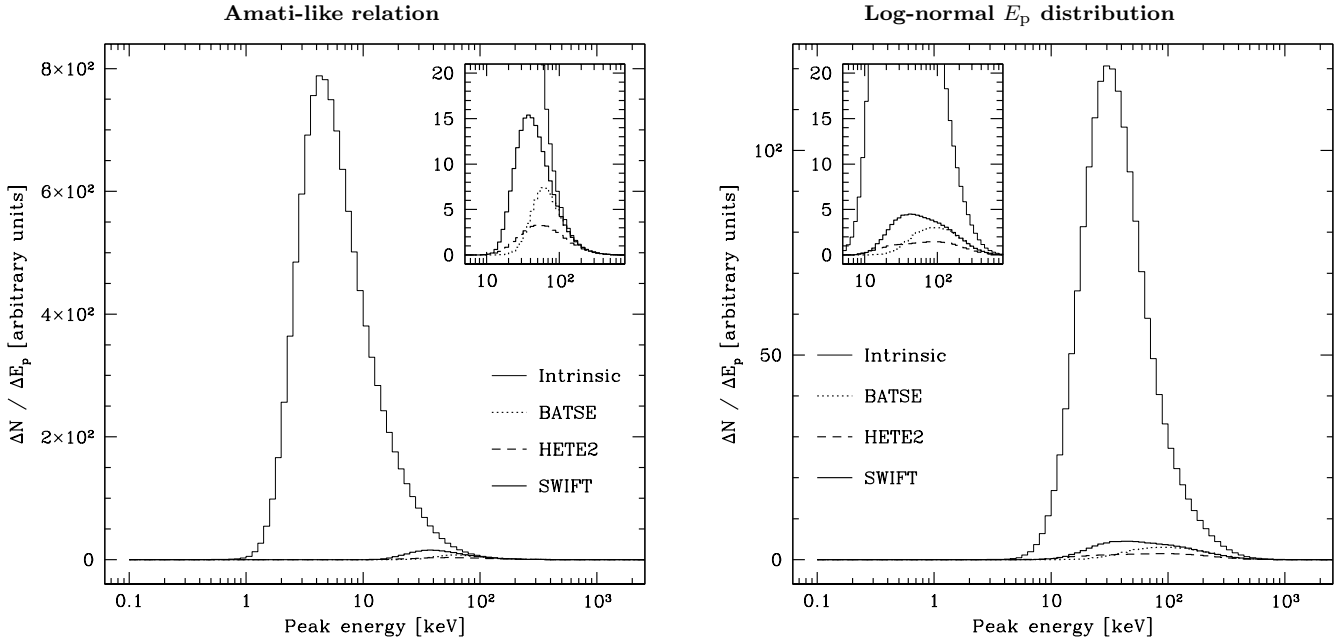


**Figure 6. Observed peak energy distribution in the best model ( $SFR_3$ ).** The peak energy distribution of all simulated GRBs, and of simulated GRBs that are detected by BATSE, HETE2 and SWIFT are plotted, insets showing with more details the regions of interest. *Left* : simulation using an Amati-like relation; *right* : simulation where the peak energy follows a log-normal distribution.



present. On the other hand, when an intrinsic correlation is assumed, detection thresholds do not modify the observed slope (left panel). This means that if the Amati relation is confirmed, it should have an intrinsic origin that should be explained by GRB models; (ii) Figure 6 shows that the intrinsic peak energy distribution is very different in the two scenarios. If an Amati-like relation is present, the intrinsic peak energy distribution is centered at about a few keV (4.5 keV for SFR<sub>3</sub>), since dim bursts are more numerous. Thus, the observed peak energy distribution in the sub-sample of bright BATSE GRBs (Preece et al. 2000) is not representative of the whole GRB population, which is largely dominated by low  $E_p$  events. On the other hand, if the peak energy distribution is not correlated with luminosity and has a log-normal distribution, then the observed distribution is close to the intrinsic distribution, centered at  $\sim 100$  keV. Notice that in both cases, the mean observed peak energy by HETE2 and SWIFT is smaller than by BATSE. This effect has also consequences on the luminosity function. As can be seen in Fig. 7, the intrinsic Amati-like relation favors the detection of low luminosity bursts, as they have a smaller peak energy and therefore more photons in the 15-150 keV band. In this scenario, the lower energy threshold (15 keV vs 25 keV) of SWIFT compared to BATSE allows SWIFT to be more efficient in sampling the luminosity function. In the log-normal  $E_p$  distribution scenario, the luminosity function of SWIFT and BATSE bursts are very similar. Notice that in both scenarios, the observed luminosity function is far from the intrinsic distribution, due to the small detection efficiency for the dimmest (most numerous) GRBs. Finally note that in the log-normal distribution case, the intrinsic mean peak energy is found to be larger than the constant value assumed by PM01.

To check the dependance of our results on the assumed shape of the luminosity function, we also made a few simulations using broken power-laws :

$$L \propto \begin{cases} L^{-0.5} & \text{for } L_{\min} \leq L \leq L_* \\ L^{-\delta} & \text{for } L_* \leq L \leq L_{\max} \end{cases} .$$

The low-luminosity slope has been fixed to avoid an additional free parameter. The value  $-0.5$  is a prediction of the internal shock model (Daigne et al. 2006). It happens that the low-luminosity branch remains mostly undetected so that the best fit parameters are very close to those obtained with a single power-law ( $L_*$  adjusting itself to the previous value of  $L_{\min}$ ). Therefore, current data do not allow to distinguish between single and broken power-laws for the GRB luminosity function.

## 5 CONCLUSION

Using Monte Carlo simulations of the long GRB population under the assumptions that (i) the GRB rate follows the SFR; (ii) the GRB luminosity function is a power-law; (iii) the peak-energy is either determined by an Amati-like intrinsic relation or by a log-normal distribution, we obtained the following results :

(i) **Luminosity function:** the slope of the power-law is

well constrained,  $\delta \sim 1.5 - 1.7$ , while the minimum and maximum luminosities are not so well determined:  $L_{\min} \sim 0.8 - 3 \times 10^{50}$  erg s<sup>-1</sup> and  $L_{\max} \sim 3 - 5 \times 10^{53}$  erg s<sup>-1</sup>. The observed distribution is very biased as most low-luminosity GRBs are not detected by current instruments.

(ii) **Intrinsic peak energy distribution:** if the observed Amati relation is confirmed, the relation needs to be intrinsic. A consequence of the relation is that the observed peak energy distribution is not representative of the whole GRB population, which has a lower mean value of a few keV. Therefore, there should be many undetected XRRs and XRFs. On the other hand, a log-normal peak energy distribution can also be in very good agreement with all the observational constraints, but selection effects alone can not produce an observed Amati relation. In this case, the mean peak energy of the whole GRB population is close to 100 keV and the observed distribution is much more representative.

(iii) **GRB comoving rate:** in agreement with Porciani & Madau (2001), we find that one GRB pointing towards us is produced every  $10^5$  to  $10^6$  supernovae in the Universe. This rate should be corrected for beaming to get the true GRB rate in the Universe. This would require to assume a distribution of beaming angle or to derive it using the observed correlation with the isotropic luminosity (Frail et al. 2001; Ghirlanda et al. 2004). The present redshift distribution of SWIFT bursts strongly favors SFR<sub>3</sub>, which still increases above  $z \sim 2$ . However, SFR<sub>3</sub> is probably unrealistic, as so many stars at high redshift would over-produce metals. This leads to conclude that *some GRBs or/and GRB progenitor properties evolve with redshift*. Our analysis suggests that the main evolutionary effect could be the redshift dependence of the efficiency of GRB production by stars, so that the GRB comoving rate still increases above  $z \sim 2$ , even if the SFR flattens or decreases. Thus, *GRBs would not directly trace the SFR*, as also suggested by recent studies on the properties of GRB host galaxies (see e.g. Le Floc'h et al. 2006). To reconcile our results with a more plausible SFR such as SFR<sub>1</sub> or even SFR<sub>2</sub>, this efficiency should be about 6 - 7 times larger at  $z = 7$  than at  $z = 2$ .

(iv) **Detection rate of high redshift GRBs:** based on a yearly rate of  $\sim 100$  SWIFT GRBs, we predict  $\sim 2 - 6$  (resp.  $\sim 1 - 5$ ) bright SWIFT bursts per year above  $z = 6$  (resp.  $z = 7$ ).

## REFERENCES

- Band D., et al., 1993, ApJ, 413, 281
- Band D. L., 2006, astro-ph/0602267
- Band D. L., Preece R. D., 2005, ApJ, 627, 319
- Berger E., Chary R., Cowie L. L., Price P. A., Schmidt B. P., Fox D. B., Cenko S. B., Djorgovski S. G., Soderberg A. M., Kulkarni S. R., McCarthy P. J., Gladders M. D., Peterson B. A., Barger A. J., 2006, astro-ph/0603689
- Blain A. W., Natarajan P., 2000, MNRAS, 312, L35
- Bloom J. S., Djorgovski S. G., Kulkarni S. R., 2001, ApJ, 554, 678
- Bouwens R. J., et al., 2003, ApJ, 595, 589
- Bouwens R. J., Illingworth G. D., Thompson R. I., Franx M., 2005, ApJL, 624, L5
- Bromm V., Loeb A., 2005, astro-ph/0509303

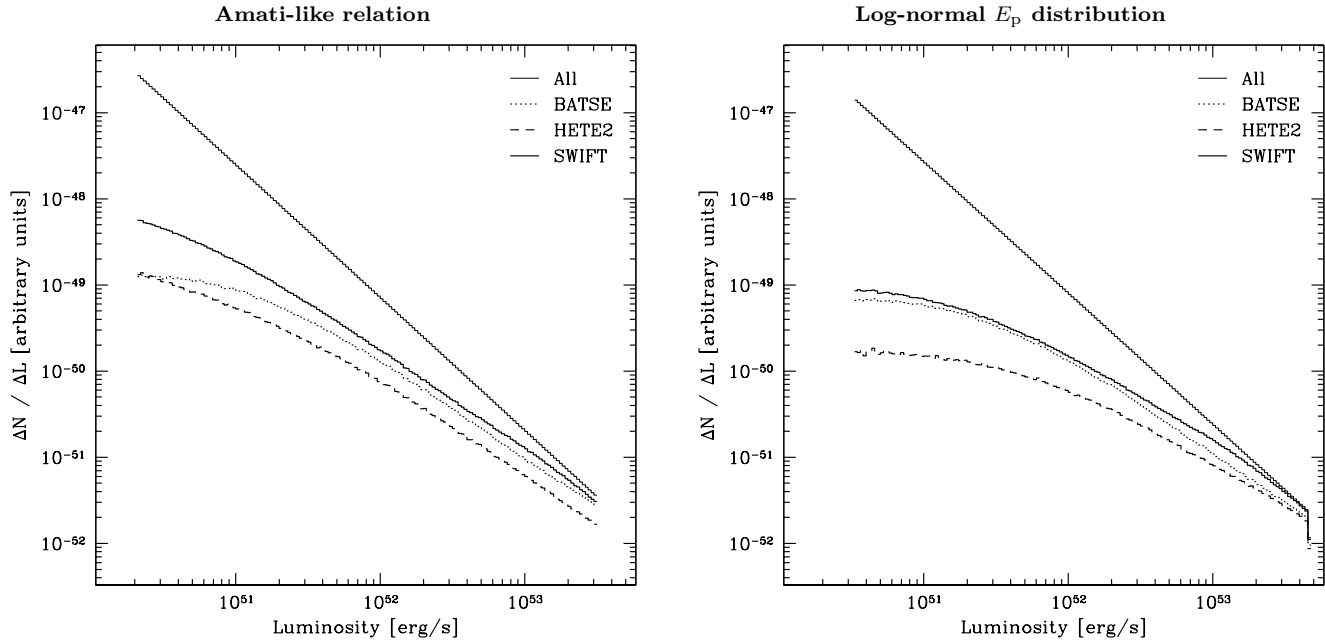


**Figure 7. Luminosity function in the best model ( $SFR_3$ ).** The intrinsic luminosity function, as well as the luminosity distribution of bursts detected by BATSE, HETE2 and SWIFT are plotted. *Left* : simulation using an intrinsic Amati-like relation; *right* : simulation where the intrinsic peak energy follows a log-normal distribution.

Chen H.-W., Prochaska J. X., Bloom J. S., 2006, astro-ph/0602144  
Daigne F., Mochkovitch R., Zitouni H., 2006, in to appear in the proceedings of the 16th Annual October Astrophysics Conference in Maryland: Gamma Ray Bursts in the Swift Era The grb luminosity function in the internal shock model  
Daigne F., Olive K. A., Silk J., Stoehr F., Vangioni E., 2005, astro-ph/0509183  
Daigne F., Olive K. A., Vangioni-Flam E., Silk J., Audouze J., 2004, ApJ, 617, 693  
Fenimore E. E., Ramirez-Ruiz E., 2000, astro-ph/0004176  
Firmani C., Avila-Reese V., Ghisellini G., Tutukov A. V., 2004, ApJ, 611, 1033  
Fontana A., Poli F., Menci N., Nonino M., Giallongo E., Cristiani S., D'Odorico S., 2003, ApJ, 587, 544  
Frail D. A., et al., 2001, ApJL, 562, L55  
Galama T. J., et al., 1998, Nat, 395, 670  
Ghirlanda G., Ghisellini G., Firmani C., Celotti A., Bosnjak Z., 2005, MNRAS, 360, L45  
Ghirlanda G., Ghisellini G., Lazzati D., 2004, ApJ, 616, 331  
Giavalisco M., et al., 2004, ApJL, 600, L103  
Guetta D., Piran T., Waxman E., 2005, ApJ, 619, 412  
Hjorth J., et al., 2003, Nat, 423, 847  
Hopkins A. M., 2004, ApJ, 615, 209  
Jakobsson P., et al., 2006, A&A, 447, 897  
Kawai N., et al., 2006, Nat, 440, 184  
Kommers J. M., Lewin W. H. G., Kouveliotou C., van Paradijs J., Pendleton G. N., Meegan C. A., Fishman G. J., 2000, ApJ, 533, 696  
Lamb D. Q., Reichart D. E., 2000, ApJ, 536, 1

Le Floch E., Charmandaris V., Forrest W. J., Mirabel F., Armus L., Devost D., 2006, astro-ph/0601251  
Malesani D., et al., 2004, ApJL, 609, L5  
Mesinger A., Perna R., Haiman Z., 2005, ApJ, 623, 1  
Nakar E., Piran T., 2005, MNRAS, 360, L73  
Natarajan P., Albanna B., Hjorth J., Ramirez-Ruiz E., Tanvir N., Wijers R., 2005, MNRAS, 364, L8  
Porciani C., Madau P., 2001, ApJ, 548, 522  
Preece R. D., Briggs M. S., Malozzi R. S., Pendleton G. N., Paciasas W. S., Band D. L., 2000, ApJS, 126, 19  
Sakamoto T., et al., 2005, ApJ, 629, 311  
Schmidt M., 1999, ApJL, 523, L117  
Stanek K. Z., et al., 2003, ApJL, 591, L17  
Stanway E. R., Bunker A. J., McMahon R. G., Ellis R. S., Treu T., McCarthy P. J., 2004, ApJ, 607, 704  
Stern B. E., Atteia J.-L., Hurley K., 2002, ApJ, 578, 304  
Stern B. E., Tikhomirova Y., Stepanov M., Kompaneets D., Berezhnoy A., Svensson R., 2000, ApJL, 540, L21  
Totani T., 1999, ApJ, 511, 41  
Wijers R. A. M. J., Bloom J. S., Bagla J. S., Natarajan P., 1998, MNRAS, 294, L13  
Yonetoku D., Murakami T., Nakamura T., Yamazaki R., Inoue A. K., Ioka K., 2004, ApJ, 609, 935